# Limit on Tensor Currents from $^8$Li $\beta$ Decay

M. G. Sternberg,[1,2,3] R. Segel,[4] N. D. Scielzo,[5,*] G. Savard,[1,2] J. A. Clark,[2] P. F. Bertone,[2,†] F. Buchinger,[6] M. Burkey,[1,2] S. Caldwell,[1,2] A. Chaudhuri,[2,7] J. E. Crawford,[6] C. M. Deibel,[8,9] J. Greene,[2] S. Gulick,[6] D. Lascar,[4,2,‡] A. F. Levand,[2] G. Li,[6,2,10] A. Pérez Galván,[2] K. S. Sharma,[7] J. Van Schelt,[1,2] R. M. Yee,[11,5] and B. J. Zabransky[2]

[1]*Department of Physics, University of Chicago, Chicago, Illinois 60637, USA*
[2]*Physics Division, Argonne National Laboratory, Argonne, Illinois 60439, USA*
[3]*Department of Physics, University of Washington, Seattle, Washington 98195, USA*
[4]*Department of Physics and Astronomy, Northwestern University, Evanston, Illinois 60208, USA*
[5]*Physical and Life Sciences Directorate, Lawrence Livermore National Laboratory, Livermore, California 94550, USA*
[6]*Department of Physics, McGill University, Montréal, Québec H3A 2T8, Canada*
[7]*Department of Physics and Astronomy, University of Manitoba, Winnipeg, Manitoba R3T 2N2, Canada*
[8]*Department of Physics and Astronomy, Louisiana State University, Louisiana 70803, USA*
[9]*Joint Institute for Nuclear Astrophysics, Michigan State University, East Lansing, Michigan 48824, USA*
[10]*Canadian Nuclear Laboratories, Chalk River, Ontario K0J 1J0, Canada*
[11]*Department of Nuclear Engineering, University of California, Berkeley, California 94720, USA*

(Received 20 March 2015; published 28 October 2015)

In the standard model, the weak interaction is formulated with a purely vector-axial-vector ($V$-$A$) structure. Without restriction on the chirality of the neutrino, the most general limits on tensor currents from nuclear $\beta$ decay are dominated by a single measurement of the $\beta$-$\bar{\nu}$ correlation in $^6$He $\beta$ decay dating back over a half century. In the present work, the $\beta$-$\bar{\nu}$-$\alpha$ correlation in the $\beta$ decay of $^8$Li and subsequent $\alpha$-particle breakup of the $^8$Be$^*$ daughter was measured. The results are consistent with a purely $V$-$A$ interaction and in the case of couplings to right-handed neutrinos ($C_T = -C_T'$) limits the tensor fraction to $|C_T/C_A|^2 < 0.011$ (95.5% C.L.). The measurement confirms the $^6$He result using a different nuclear system and employing modern ion-trapping techniques subject to different systematic uncertainties.

DOI: 10.1103/PhysRevLett.115.182501 PACS numbers: 23.40.Bw, 37.10.Mn, 37.10.Ty

The most general form of the electroweak theory contains couplings $C_i$ and $C_i'$ for each possible interaction type [$i$ = scalar ($S$), vector ($V$), axial-vector ($A$), tensor ($T$), or pseudoscalar ($P$)]. $C_i$ and $C_i'$ differ in the form of the interaction by a factor of $\gamma_5$ allowing for parity violation [1]. The differing chiral properties of the interactions lead to different angular correlations in nuclear $\beta$ decay, and this fact was used to help establish the left-handed $V$-$A$ nature of the weak interaction in the late 1950s and early 1960s [2–4]. Why the weak interaction maximally violates parity with such a preferred handedness is one of the great outstanding questions of modern physics.

Various extensions to the standard model (SM) allow for right-handed currents as well as $S$, $T$, and $P$ interactions to emerge [5,6]. Of the non-standard-model interactions, the limits on $T$ are the weakest. If no assumption is made about the chirality of the neutrino, global analysis of the available nuclear and neutron $\beta$-decay data yields $|C_T/C_A| < 0.081$ at 95.5% C.L. for $C_T = -C_T'$ [7,8]. For simplicity, we assume throughout the Letter that $C_T = -C_T'$ and $C_A = C_A'$, a constraint that will be relaxed in the final conclusion. If one considers only left-handed neutrinos (i.e., $C_T = C_T'$), then the aforementioned constraint becomes more stringent by more than an order of magnitude. The limit on $|C_T/C_A|$ is strongly influenced by a 1963 measurement of the $\beta$-$\bar{\nu}$ correlation $a_{\beta\nu}$ in the decay of $^6$He [2,9].

Recent technological developments in both neutral and ion traps have made possible a new generation of $\beta$-decay experiments in which the parent nuclei decay nearly at rest in a small, well-localized volume from which the decay products emerge essentially free from scattering. Measurements of $a_{\beta\nu}$ using atom traps have achieved a relative precision at or below 1% for Fermi ($a_{\beta\nu} = 1$) and mixed transitions [10,11], while experiments investigating Gamow-Teller ($a_{\beta\nu} = -1/3$) decays within ion traps have reached a few percent precision [12,13].

This work builds upon previous efforts using trapped ions [13] and presents a limit on weak tensor currents comparable to that from the most precise angular correlation measurement in a pure Gamow-Teller decay [2]. The limit has been determined from the $\beta$ decay of $^8$Li from the $J^\pi = 2^+$ $I_z = 1$ ground state to the broad $J^\pi = 2^+$ $I_z = 0$ excited state in $^8$Be. *Ab initio* calculations have confirmed that the transition is predominantly Gamow-Teller with isospin mixing of a Fermi contribution limited to less than $10^{-3}$ [14] and therefore below the sensitivity of this work. The $^8$Be$^*$ daughter nucleus immediately breaks up into two $\alpha$ particles, the energies of which are boosted in the laboratory frame due to the momentum imparted from $\beta$ decay.

 

The $^8$Li system has several features that make it an exceptional candidate for studying $\beta$-decay angular correlations. The large $Q$ value and light mass result in large nuclear-recoil energies, and the delayed $\alpha$ particles are emitted in an easy-to-detect ~MeV energy range, while symmetries within the detector array suppress a number of systematic effects. The $^8$Be$^*$ recoils with energies up to 12 keV leading to energy differences between coincident $\alpha$ particles in excess of 400 keV. Finally, the angular distribution of the $\bar{\nu}$ is correlated not only with the direction of the $\beta$ but also with the angle between the $\beta$ and the $\alpha$ breakup axis [15,16]. For decays in which the $\beta$ is emitted along the $\alpha$ breakup axis, the $\beta$-$\bar{\nu}$-$\alpha$ correlation leads to a factor of 3 enhancement in sensitivity to tensor currents.

In the allowed approximation, the $\beta$-decay rate for nuclei undergoing delayed $\alpha$-particle emission, averaged over a uniform distribution of nuclear polarizations, is given by [16]

$$W \propto F(Z,E_e)p_eE_e(E_0-E_e)^2\left[g_1+g_2\frac{\vec{p}_e\cdot\vec{p}_\nu}{E_eE_\nu}+b\frac{m_e}{E_e}+g_{12}\left(\frac{(\vec{p}_e\cdot\hat{\alpha})(\vec{p}_\nu\cdot\hat{\alpha})}{E_eE_\nu}-\frac{1}{3}\frac{\vec{p}_e\cdot\vec{p}_\nu}{E_eE_\nu}\right)\right], \quad (1)$$

where $F(Z,E_e)$ is the Fermi function, $(E_e,\vec{p}_e)$ and $(E_\nu,\vec{p}_\nu)$ are the $\beta$ and $\bar{\nu}$ four-momenta, respectively, $E_0$ is the end-point energy, $m_e$ is the electron mass, $\hat{\alpha}$ is the $\alpha$-particle-momentum unit vector, and $b$ is the Fierz interference term. General limits on $b$ for Gamow-Teller decays are of the order of ~0.01 [17,18], and this term vanishes for $C_T=-C_T'$.

The $\beta$-$\bar{\nu}$ correlation parameter $a_{\beta\nu}\equiv g_2/g_1$ can be related to $g_{12}/g_1$ after consideration of the spins of the nuclei involved in the $\beta$ decay and delayed-$\alpha$ emission process. For a $2^+\to 2^+\to 0^+$ spin sequence, this yields

$$a_{\beta\nu}=\frac{1}{3}\frac{g_{12}}{g_1}=\frac{1}{3}\frac{|C_T|^2-|C_A|^2}{|C_T|^2+|C_A|^2}. \quad (2)$$

Using this relation in Eq. (1), one can see that, if $(\vec{p}_e\cdot\hat{\alpha})=0$, the effective $\beta$-$\bar{\nu}$ correlation vanishes, whereas $(\vec{p}_e\cdot\hat{\alpha})=1$ results in an effective correlation parameter of $3a_{\beta\nu}$. Therefore, decays in which the $\beta$ is emitted approximately parallel to an $\alpha$ have an enhanced sensitivity to tensor currents. Radiative and recoil-order corrections give rise to $E_e$-dependent perturbations of the form factors $g_1$, $g_2$, and $g_{12}$ and additional correlations between the $\beta$, $\bar{\nu}$, and $\alpha$ particles.

The $^8$Li was produced via the $^7$Li$(d,p)^8$Li stripping reaction at the Argonne Tandem-Linac Accelerator System (ATLAS). Details of the production and subsequent stopping of the reaction products within the gas catcher can be found in Ref. [13]. Ions were extracted from the gas catcher as $^8$LiOH$^+$ and entered an ion injection system [19], where ions were bunched, cooled, and delivered to a preparation gas-filled Penning trap [20]. Resonant excitation of the molecular ions within the preparation trap broke them up into $^8$Li$^+$ ions through buffer-gas collisions with near 100% efficiency. The $^8$Li$^+$ ions were then transported to the Beta-Decay Paul Trap (BPT) [21] where the decay correlation measurement ensued.

The BPT is a linear Paul trap constructed with thin planar electrodes that provide an open geometry to allow large solid-angle detector coverage (Fig. 1). Ion confinement within the radial plane of the trap was achieved by applying a radio frequency (rf) voltage of ~700 $V_{pp}$ at 1.3 MHz which produced a radial confining pseudopotential of approximately 5 V/cm$^2$. The ions were confined axially with a harmonic confining potential of ~3 V/cm$^2$. The ions were thermalized using $\sim 10^{-5}$ torr buffer gas of high-purity helium cooled to ~90 K by circulating liquid nitrogen through the support frame of the trap.

The BPT detector system has undergone a substantial upgrade since the work presented in Ref. [13]. The original setup consisted of four sets of silicon detectors with each set containing a $50\times 50\times 0.30$ mm$^3$ double-sided silicon detector (DSSD) with 16 strips on each side backed by three $50\times 50\times 1$ mm$^3$ single-element silicon detectors (SDs). The DSSDs were used to detect the $\alpha$ particles, and the SDs were used to detect the $\beta$ particles. In the current configuration, each DSSD-SD detector set has been replaced by a single $64\times 64\times 1$ mm$^3$ DSSD with 32 strips on each side and dead layers ~5 times thinner than those on the previous DSSDs. The 95%-transmission nickel mesh screen in front of the detectors, previously used to shield the detectors from rf interference, was removed, and instead an additional layer of rf shielding was added with an

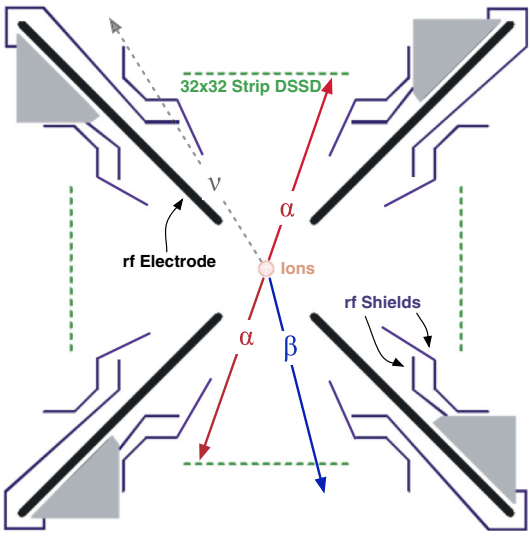


FIG. 1 (color online). Cross-sectional view of the BPT and detector system in the rf plane. The direction of the emitted $\alpha$'s and $\beta$'s is determined by the vector between the trap center and detector pixels.

opening to allow the $\alpha$ and $\beta$ particles to reach the detector unobstructed.

With the 1-mm-thick DSSDs, both $\alpha$ and $\beta$ particles can be identified by their energy deposition within a single detector pixel. The $\beta$ particles deposit ~300 keV in the 1-mm-thick DSSDs with a high-energy tail that extends into the region of the $\alpha$ spectrum above 500 keV. The observation of distinct $\beta$ and $\alpha$ hits in separate pixels eliminates summing.

The amplifier noise and rf pickup on the detectors were reduced to a level that resulted in an energy resolution better than 20 keV for most strips, a factor of 2.5 improvement compared to earlier work. However, over half of the strips on the left and right detectors and nine strips from the top and bottom detectors were unusable due to noise issues. The outermost strips of each detector were also excluded from the analysis due to incomplete charge collection at the edges of the detectors. In total, 23 of 64 strips were used from the left and right detectors and 51 of 64 strips from the top and bottom detectors.

The linearity of the detector system was monitored with the use of a precision pulser that coupled a fixed amount of charge onto each silicon strip. An absolute energy calibration of each strip was continually performed *in situ* throughout the experiment using $^{148}$Gd and $^{244}$Cm sources that emit $\alpha$ particles at 3182.690(24) and 5804.77(5) keV, respectively [22,23]. The sources were mounted on the inner rf shields and illuminated all of the strips facing the trapped ion cloud. The $\alpha$-source lines were combined with the pulser data to provide a precision calibration up to 6 MeV, following corrections to account for the detector dead layer and nonionizing energy losses within the silicon.

With a trapped cloud maintained at ~20 $^8$Li ions, approximately $1.2 \times 10^6$ $\alpha$-$\alpha$ coincidences and $3 \times 10^5$ $\beta$-$\alpha$-$\alpha$ coincidences were measured over the course of 7 days, prior to analysis cuts. Comparison of the relative position between coincident $\alpha$ events on the detectors provided an effective image of the ion cloud [21]. After 20 ms postinjection, the ion cloud was found to be within 10% of its equilibrium size. The ion-cloud extent was found to be roughly the same in all three dimensions and was approximated by a spherical Gaussian distribution with a FWHM of 1.8 mm.

Events were selected for analysis if (i) the ions had more than 20 ms in the trap to thermally equilibrate, (ii) two $\alpha$ particles were observed with energies between 750 and 5000 keV, (iii) a $\beta$ was identified with between 200 and 700 keV deposited in the silicon, and (iv) the energy collected in the front and back strips for each particle agreed to within 50 keV. The last requirement minimizes the systematic effect from $\alpha$ particles that hit the gap between adjacent front strips [24].

A detailed Monte Carlo simulation was developed to model the decays of $^8$Li within the trap environment. In order to achieve the desired precision, it is necessary to accurately account for the $\beta$-decay kinematics, the geometry of the apparatus, the solid-angle coverage of the detectors, and the detector response. The $\beta$-decay event generator described in Refs. [11,25] was modified to include the broad $^8$Be$^*$ final state distribution sampled according to Ref. [26]. Correlation terms up to order $E_e/M_{\mathrm{Li}}$, and the $(E_e/M_{\mathrm{Li}})^2$ and order-$\alpha Z$-dependent radiative corrections to these terms, were included [27] according to the prescription of Ref. [16]. $Z$-independent radiative corrections were also included according to the prescription given in Ref. [28] after being modified to include the effects of delayed-$\alpha$ emission. The simulation was developed within the GEANT4 framework [29] (with the trap geometry imported from Autodesk Inventor using a GDML toolkit [30]) to incorporate the effects of $\beta$ scattering. Decay spectra for pure axial-vector and pure tensor decays are generated for comparison with the experimental results.

Triple coincident $\beta$-$\alpha$-$\alpha$ events in which the $\beta$ was detected in the same detector as one of the $\alpha$ particles were used to make four $\alpha$ energy-difference spectra, one for each possible $\beta$ direction (top, bottom, left, and right). Because the $\beta$-$\alpha$-$\alpha$ events are kinematically complete, it is also possible to reconstruct the angle $\theta_{\beta\nu}$ between the $\beta$ and $\bar{\nu}$ on an event-by-event basis. However, the $\cos(\theta_{\beta\nu})$ spectra are more susceptible to uncertainties in the size of the ion cloud and have poorer sensitivity compared to the energy-difference spectra due to the angular resolution of the reconstructed momenta.

The experimental spectra are fit to a linear combination of the simulated pure $A$ and $T$ spectra with the only free parameter being the relative amplitudes of the couplings $|C_T/C_A|^2$. Figure 2 shows the combined energy-difference and $\cos(\theta_{\beta\nu})$ fit results from the top-bottom detector pair with the $\beta$ detected on the top or bottom detector. Combining the results from all four energy-difference spectra gives $|C_T/C_A|^2 = -0.0013 \pm 0.0038_{\mathrm{stat}}$ and is consistent with the results from the $\cos(\theta_{\beta\nu})$ spectra.

The dominant $1\sigma$ systematic uncertainties for the $\alpha$ energy-difference fits are listed in Table I. The systematics are expected to be independent, and the total is calculated by summing each component in quadrature. A brief description of the dominant systematic effects follows.

*Energy calibration.*—The systematic uncertainty introduced from the energy calibration is dominated by uncertainties in the linear slope of the calibration. Averaging the results of the energy-difference spectral fits from all four detectors suppresses this systematic effect by about an order of magnitude, though the suppression is slightly diminished due to dead or rejected strips.

The energy-calibration slope is determined from the *in situ* calibration sources combined with the pulser data. The $\alpha$ peaks were fit with a skewed Gaussian distribution of the form given in Ref. [26], and the absolute energy was determined offline by a comparison of these source spectra

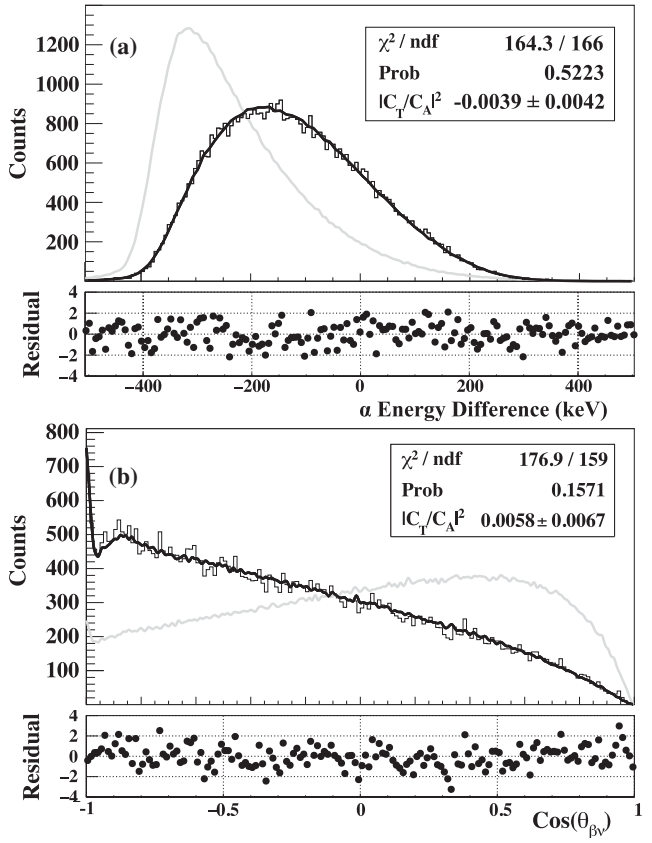


FIG. 2. Spectra from events with $\beta$ and $\alpha$ particles detected on the top and bottom detector. (a) Energy difference along with the fit to the simulated spectrum and the normalized residual. (b) The reconstructed $\cos(\theta_{\beta\nu})$ spectrum for the same events with a fit to the simulated spectrum and the normalized residual. The gray curves show the expected spectra for a pure $T$ interaction.

with spectra taken using thin spectroscopy-grade $\alpha$ sources. The weighted average uncertainty in the slope from all four detectors was 0.1%, with the dominant source of error coming from uncertainties in the fit of the *in situ* calibration $\alpha$ peaks. The total energy calibration systematic uncertainty is 0.0013 on $|C_T/C_A|^2$.

*$\alpha$ line shape.*—The $\alpha$ particle line shape was modeled based on the detector response to thin precision $\alpha$ sources. Changes in the detector response during the experiment were monitored with the *in situ* calibration sources. Comparison of the high-energy side half widths of the *in situ* sources were found to agree with the precision thin sources to within 10%. Varying the widths of the simulated line shapes by 10% led to a maximum shift in $|C_T/C_A|^2$ of 0.0018.

*Silicon dead layer and energy defects.*—The dead layers were determined offline by measuring the charge collected on the silicon detectors from thin $\alpha$ sources entering the detector at various angles and comparing the results with stopping powers (and energy losses due to nonionizing processes) calculated using the Stopping and Range of Ions in Matter (SRIM) program [31]. The results for all four detectors were consistent with a dead layer of $115 \pm 4$ nm leading to an uncertainty on $|C_T/C_A|^2$ of 0.0008.

*$\beta$ scattering.*—The effects of $\beta$ scattering have been modeled within GEANT4 [29] using the PENELOPE physics models [32,33] along with the Goudsmit-Saunderson multiple-scattering model [34,35]. Inclusion of $\beta$ scattering led to a correction on $|C_T/C_A|^2$ of 0.013. The accuracy of the GEANT4 simulations was benchmarked against experimental observables such as the number of backscattered $\beta$ particles detected coincidentally on opposite-facing detectors. The simulations agree within the statistical uncertainty of the data. The GEANT4 simulation is estimated to have an accuracy of 15% at these energies, and an uncertainty of 0.0020 is assigned to $|C_T/C_A|^2$ accordingly.

*Backgrounds.*—No events met the criteria for a true $\beta$-$\alpha$-$\alpha$ coincidence during the background measurements with the BPT emptied. However, the background measurements only occurred every 27 s and lasted for only 120 ms. This leads to a limit on the possible number of false $\beta$-$\alpha$-$\alpha$ coincidences of $< 230$ due to backgrounds. This corresponds to an uncertainty on $|C_T/C_A|^2$ of 0.0011.

*Recoil and radiative corrections.*—The largest recoil-order corrections arise from the second-forbidden $j_2$ and $j_3$ terms, which shift $|C_T/C_A|^2$ by $-0.011$. Because of the relatively large uncertainty in $j_2$ and $j_3$ as measured by Ref. [36], the corrections have an uncertainty on $|C_T/C_A|^2$ of 0.0025. The combined effect of the weak magnetism and induced tensor terms $b_M$ and $d^I$ are comparatively smaller and give rise to an uncertainty on $|C_T/C_A|^2$ of 0.0006. $Z$-independent radiative corrections, including effects arising from bremsstrahlung emission in the final state, lead to a correction on $|C_T/C_A|^2$ of 0.0059 with an associated 10% uncertainty. The combined uncertainty from the recoil and radiative corrections is 0.0026.

*Nondominant systematic uncertainties.*—The energy threshold for determining if an event is a $\beta$ or $\alpha$ was chosen to minimize the number of false particle identifications. Varying this parameter by $\pm 100$ keV led to a maximum shift in $|C_T/C_A|^2$ of 0.0006. Additional systematic errors such as those from stray magnetic fields, perturbation in trajectories due to trap voltages, or the temperature of the ion cloud contribute at a level of 0.0001 on $|C_T/C_A|^2$. The sum of

TABLE I. Dominant sources of systematic uncertainty at $1\sigma$.

| Source | $\Delta\lvert C_T/C_A\rvert^2$ |
|---|---|
| Energy calibration | 0.0013 |
| $\alpha$ line shape | 0.0018 |
| Dead layer thickness | 0.0008 |
| $\beta$ scattering | 0.0020 |
| Backgrounds | 0.0011 |
| Recoil and radiative | 0.0026 |
| Nondominant systematics | 0.0007 |
| Total | 0.0043 |

the nondominant systematic effects lead to a combined uncertainty of 0.0007 in $|C_T/C_A|^2$ at $1\sigma$.

The combined results of the four fits yield

$$|C_T/C_A|^2 = -0.0013 \pm 0.0038_{\text{stat}} \pm 0.0043_{\text{syst}} \quad (3)$$

with the uncertainties given at $1\sigma$. Using a Bayesian approach with a uniform prior for $|C_T/C_A|^2 > 0$ leads to a limit on tensor couplings of $|C_T/C_A|^2 < 0.011$ or $|C_T/C_A| < 0.10$ (95.5% C.L.) [37]. Equivalently, the results can be expressed as $a_{\beta\nu} = -0.3342 \pm 0.0026_{\text{stat}} \pm 0.0029_{\text{syst}}$ or $g_{12}/g_1 = -1.003 \pm 0.008_{\text{stat}} \pm 0.009_{\text{syst}}$ (at $1\sigma$). Both $a_{\beta\nu}$ and $g_{12}/g_1$ agree with the expected SM values of $-1/3$ and $-1$, respectively, and corroborate the results of the long-standing $^6$He $a_{\beta\nu}$ measurement [2]. The results presented here are given in terms of $|C_T/C_A|^2$ with the additional constraint that $C_T = -C_T'$. This constraint can be lifted, in which case the results for $a_{\beta\nu}$ can be replaced with $\tilde{a}_{\beta\nu} \equiv a_{\beta\nu}/(1 + bm_e/\langle E_e\rangle)$, where $\langle E_e\rangle$ is the average $\beta$ energy in the decay and $m_e/\langle E_e\rangle = 0.070$.

The same techniques used here can be applied to $^8$B, the mirror nucleus of $^8$Li, allowing for precision tests of the conserved-vector-current hypothesis and searches for second-class currents. Upgrades to the production and transport of radioactive ions have already been implemented which will allow for roughly an order of magnitude improvement in the number of trapped $^8$Li ions. Online production and trapping of $^{20}$Na is being investigated as a potential trapped calibration $\alpha$ source that would provide a zero thickness source to better characterize the detector response over a range of 700 keV to 5.7 MeV.

We acknowledge the ATLAS staff for their help and support. We thank Dariusz Seweryniak and Calem Hoffman for lending us electronics and providing technical advice. The authors are grateful for discussions with Frederik Wauters on the interpretation of the results of the experiment. This work was carried out under the auspices of the NSERC, Canada, Application No. 216974, and the U.S. Department of Energy, by Argonne National Laboratory under Contract No. DE-AC02-06CH11357 and Lawrence Livermore National Laboratory under Contract No. DE-AC52-07NA27344. This research used resources of Argonne National Laboratory's ATLAS facility, which is a DOE Office of Science User Facility.

*Corresponding author.
scielzo1@llnl.gov
†Present address: Marshall Space Flight Center, Huntsville, Alabama 35812, USA.
‡Present address: TRIUMF, Vancouver, British Columbia V6T 2A3, Canada.

[1] T. D. Lee and C. N. Yang, Phys. Rev. **104**, 254 (1956).
[2] C. H. Johnson, F. Pleasonton, and T. A. Carlson, Phys. Rev. **132**, 1149 (1963).
[3] R. P. Feynman and M. Gell-Mann, Phys. Rev. **109**, 193 (1958).
[4] E. C. G. Sudarshan and R. E. Marshak, Phys. Rev. **109**, 1860 (1958).
[5] P. Herczeg, Prog. Part. Nucl. Phys. **46**, 413 (2001).
[6] S. Profumo, M. J. Ramsey-Musolf, and S. Tulin, Phys. Rev. D **75**, 075017 (2007).
[7] N. Severijns, M. Beck, and O. Naviliat-Cuncic, Rev. Mod. Phys. **78**, 991 (2006).
[8] F. Wauters, A. García, and R. Hong, Phys. Rev. C **89**, 025501 (2014).
[9] F. Glück, Nucl. Phys. **A628**, 493 (1998).
[10] A. Gorelov, D. Melconian, W. P. Alford, D. Ashery, G. Ball, J. A. Behr, P. G. Bricault, J. M. D'Auria, J. Deutsch, J. Dilling, M. Dombsky, P. Dubé, J. Fingler, U. Giesen, F. Glück, S. Gu, O. Häusser, K. P. Jackson, B. K. Jennings, M. R. Pearson, T. J. Stocki, T. B. Swanson, and M. Trinczek, Phys. Rev. Lett. **94**, 142501 (2005).
[11] P. A. Vetter, J. R. Abo-Shaeer, S. J. Freedman, and R. Maruyama, Phys. Rev. C **77**, 035502 (2008).
[12] X. Fléchard, P. Velten, E. Liénard, A. Méry, D. Rodríguez, G. Ban, D. Durand, F. Mauger, O. Naviliat-Cuncic, and J. C. Thomas, J. Phys. G **38**, 055101 (2011).
[13] G. Li, R. Segel, N. D. Scielzo, P. F. Bertone, F. Buchinger, S. Caldwell, A. Chaudhuri, J. A. Clark, J. E. Crawford, C. M. Deibel, J. Fallis, S. Gulick, G. Gwinner, D. Lascar, A. F. Levand, M. Pedretti, G. Savard, K. S. Sharma, M. G. Sternberg, T. Sun, J. Van Schelt, R. M. Yee, and B. J. Zabransky, Phys. Rev. Lett. **110**, 092502 (2013).
[14] R. B. Wiringa, S. Pastore, S. C. Pieper, and G. A. Miller, Phys. Rev. C **88**, 044333 (2013).
[15] M. Morita, Phys. Rev. Lett. **1**, 112 (1958).
[16] B. R. Holstein, Rev. Mod. Phys. **46**, 789 (1974).
[17] B. R. Holstein, Phys. Rev. C **16**, 753 (1977).
[18] A. S. Carnoy, J. Deutsch, T. A. Girard, and R. Prieels, Phys. Rev. C **43**, 2825 (1991).
[19] J. Fallis, Ph.D. thesis, University of Manitoba, 2009.
[20] G. Savard, S. Becker, G. Bollen, H.-J. Kluge, R. Moore, T. Otto, L. Schweikhard, H. Stolzenberg, and U. Wiess, Phys. Lett. A **158**, 247 (1991).
[21] N. Scielzo, G. Li, M. Sternberg, G. Savard, P. Bertone, F. Buchinger, S. Caldwell, J. Clark, J. Crawford, C. Deibel, J. Fallis, J. Greene, S. Gulick, A. Hecht, D. Lascar, J. Lee, A. Levand, M. Pedretti, R. Segel, H. Sharma, K. Sharma, I. Tanihata, J. V. Schelt, R. Yee, and B. Zabransky, Nucl. Instrum. Methods Phys. Res., Sect. A **681**, 94 (2012).
[22] Y. A. Akovali, Nucl. Data Sheets **84**, 1 (1998).
[23] B. Singh and E. Browne, Nucl. Data Sheets **109**, 2439 (2008).
[24] J. Yorkston, A. Shotter, D. Syme, and G. Huxtable, Nucl. Instrum. Methods Phys. Res., Sect. A **262**, 353 (1987).
[25] N. D. Scielzo, S. J. Freedman, B. K. Fujikawa, and P. A. Vetter, Phys. Rev. Lett. **93**, 102501 (2004).
[26] M. Bhattacharya, E. G. Adelberger, and H. E. Swanson, Phys. Rev. C **73**, 055802 (2006).
[27] Equation (53) of Ref. [16] requires a correction in the sequential numbering of spectral functions $g_{11}$ through $g_{15}$:

the second instance of $g_{11}$ should be $g_{12}$, $g_{12}$ should be $g_{13}$, and $g_{13}$ should be $g_{14}$.

[28] F. Glück, Comput. Phys. Commun. **101**, 223 (1997).

[29] A. Agostinelli *et al.*, Nucl. Instrum. Methods Phys. Res., Sect. A **506**, 250 (2003).

[30] http://cad-gdml.in2p3.fr/.

[31] J. F. Ziegler, M. Ziegler, and J. Biersack, Nucl. Instrum. Methods Phys. Res., Sect. B **268**, 1818 (2010).

[32] F. Salvat *et al.*, *Penelope: A Code System for Monte Carlo Simulation of Electron and Photon Transport, data bank* (OECD Nuclear Energy Agency, 2001).

[33] I. Kawrakow and A. F. Bielajew, Nucl. Instrum. Methods Phys. Res., Sect. B **134**, 325 (1998).

[34] S. Goudsmit and J. L. Saunderson, Phys. Rev. **57**, 24 (1940).

[35] O. Kadri, V. Ivanchenko, F. Gharbi, and A. Trabelsi, Nucl. Instrum. Methods Phys. Res., Sect. B **267**, 3624 (2009).

[36] T. Sumikama, K. Matsuta, T. Nagatomo, M. Ogura, T. Iwakoshi, Y. Nakashima, H. Fujiwara, M. Fukuda, M. Mihara, K. Minamisono, T. Yamaguchi, and T. Minamisono, Phys. Rev. C **83**, 065501 (2011).

[37] K. A. Olive *et al.*, Chin. Phys. C **38**, 090001 (2014).